Phase transitions of extended-range probabilistic cellular automata with two absorbing states

Franco Bagnoli*
Dipartimento di Energetica, Università di Firenze, Via S. Marta 3, 50139 Firenze, Italy

Fabio Franci†
Dipartimento di Matematica Applicata, Università di Firenze, Via S. Marta 3, 50139 Firenze, Italy

Raúl Rechtman‡
Centro de Investigación en Energía, Universidad Nacional Autónoma de México, Apartado. Postal 34, 62580 Temixco, Morelos, Mexico
(Received 26 May 2004; revised manuscript received 31 October 2004; published 7 April 2005)

We study phase transitions in a long-range one-dimensional cellular automaton with two symmetric absorbing states. It includes and extends several other models, like the Ising and Domany-Kinzel ones. It is characterized by competing ferromagnetic linear and antiferromagnetic nonlinear couplings. Despite its simplicity, this model exhibits an extremely rich phase diagram. We present numerical results and mean-field approximations.

DOI: 10.1103/PhysRevE.71.046108 PACS number(s): 05.50.+q, 68.35.Rh, 64.60.−i

I. INTRODUCTION

Simple discrete models are valuable tools for exploring phase transitions, both in equilibrium and out of equilibrium. A paradigmatic example of the first kind is the kinetic Ising model (heat-bath dynamics), which can be formulated as a probabilistic cellular automaton (PCA) (see Appendix and Ref. [1]). One of the simplest examples of a system exhibiting out of equilibrium phase transitions is the Domany-Kinzel (DK) model [2], which is a natural extension of the directed percolation (DP) problem in the language of cellular automata.

Frustration plays a central role in characterizing the phase diagrams of many simple models. One can have geometric frustration, as in a triangular antiferromagnetic Ising model, or fluctuating coupling, as in spin glasses [3] or *p*-spin models [4]. In this latter model, even a flip of a single spin may change the interaction between ferromegnetic and antiferromagnetic. We discuss here a simpler one-dimensional model in which frustration plays a central role. This model is a variation of the droplet model in which the particles tend to repel each other when they are dispersed but in which clusters, once formed, cannot break and only particles near the surface can eventually leave them.

The model originated from the schematization of the mechanism of opinion formation in a homogeneous (no leader) society [5], in which it was assumed that a coherent local community exerts a very strong social pressure on an individual's opinion. However, there is the possibility of disagreement with a weak local majority depending on the individual's education. In the case of a diffuse nonconformistic attitude, people tend to act in the opposite way to the local majority (antiferromagnetic coupling), introducing frustration. The presence of absorbing states may cause the formation of large coherent clusters, whose interactions give rise to interesting patterns.

This model could also be applied to a system of charged, magnetized metallic particles. These repel each other due to their charge, but are attracted due to their magnetic coupling. With a proper choice of parameters, one may have repulsion when particles are scattered. However, once a cluster of particles in contact appears, the mobility of charges may reduce the electric force between this cluster and an external particle, and the interaction may become attractive. Other examples can be found in aggregation models.

In what follows, we discuss a one-dimensional spin model characterized by two coupling factors; one that behaves like the Ising (magnetic) coupling, i.e., for a given spin, grows linearly with the local field, and a *nonlinear term*, which is very low for a weak local field, but grows quickly when the local field exceeds a certain threshold.

In one dimension, no true phase transition appears for finite-range and finite-strength coupling. On the other hand, models presenting absorbing states, like the DK one, do exhibit nonequilibrium phase transitions. The presence of absorbing states may be related to the divergence of some coupling, which becomes infinite (see Appendix and Ref. [1]). Thus, in our model, we simply assume a two-level nonlinear coupling: zero for local field below a given threshold (corresponding to the parameter Q in the following) and infinite otherwise. Thus, in total we have four parameters: the range R, the external magnetic field H and local coupling J as in the Ising model, and the threshold Q. We denote these models by RQ, indicating the range and the threshold, say, $R3Q1$, $R5Q2$, and so on.

The model can also be discussed as a one-dimensional probabilistic cellular automaton. In this guise, it may be considered an extension of the DK model, or, more precisely, of

*Also at INFN, sez. Firenze and Centro Interdipartimentale per lo Studio di Dinamiche Complesse, Università di Firenze, Firenze, Italy; Electronic address: franco.bagnoli@unifi.it

†Also at Centro Interdipartimentale per lo Studio di Dinamiche Complesse, Università di Firenze, Firenze, Italy; Electronic address: fabio.franci@unifi.it

‡Electronic address: rrs@cie.unam.mx

the $R3Q1$ model [6]. This model exhibits a richer phase diagram than the DK one, and we shall show that for $R\to\infty$, the RQ model presents different features, like a disorder-chaotic transition.

It is not surprising that frustration gives rise to disordered behavior, which may be sometimes considered chaotic from a microscopic point of view. We investigate this aspect using an original chaotic observable, corresponding to a finite-distance Lyapunov exponent. However, when renormalized (or locally averaged), a *disordered* behavior simply corresponds to a stable almost-zero magnetization. In the mean-field approximation, it corresponds to a fixed point of observables. In our model also a coherently chaotic phase appears, in which large patches of sites oscillate wildly, corresponding to a chaotic map in the mean-field approximation.

In summary, we observe that the *usual* transitions from ordered into active phases become much richer, being preceded by a transition from coherently chaotic to simply chaotic, then to more irregular states, the appearance of a parameter-insensitive disordered phase, and finally an *escape* to ordered (quiescent) states with a discontinuous (first-order) character. The origin of this behavior is the competition between linear antiferromagnetic and nonlinear ferromagnetic couplings.

The paper is organized as follows. In Sec. II we present the RQ model as both a spin system and a PCA. In Sec. III we present numerical results of the model beginning with a review of the simplest nontrivial case $R=3$, $Q=1$, and Sec. IV is devoted to a mean-field discussion of the model. The paper ends with some conclusions.

II. THE MODEL

Both the kinetic Ising model (see Appendix) and the DK one are Boolean, one-dimensional, $R=2$ PCA's in which the state of a given cell depends probabilistically on the sum S of the states of its two nearest neighbors at the previous time step. That is, there are three different conditional probabilities $\tau(1|S)$, $S=0,1,2$, that the future state of the cell is 1 given S neighbors in state 1. In the DK model $\tau(1|0)=0$ which means that there is an absorbing phase corresponding to the configuration where the state on every cell is zero. The presence of more than one absorbing state can induce different behaviors and trigger the appearance of universality classes different from the usual directed percolation one [7–9].

We denote by $s_i^t\in\{0,1\}$ the state at site $i=0,\ldots,L-1$ and time $t=1,2,\ldots,T$. All operations on spatial indices are assumed to be modulo L (periodic boundary conditions). The range of interactions is denoted by R, that is, s_i^{t+1} depends on the states at time t in a neighborhood $\mathcal{N}_i$ that contains the R nearest neighbors of site i. It is convenient to introduce also the spin notation $\sigma_i^t=2s_i^t-1$, $\sigma_i^t\in\{-1,1\}$.

The spin σ_i^t experiences the local field $V(m_i^t)=H+[J+K(m_i^t)]m_i^t$, where H is an external field, J a coupling constant, and m_i^t the local magnetization defined by

$$m_i^t=\sum_{j\in\mathcal{N}_i}\sigma_j^t=2S_i^t-R,$$

where

$$S_i^t=\sum_{j\in\mathcal{N}_i}s_j^t.$$

The presence of absorbing states is due to a nonlinear coupling K given by

$$K(m)=K(m(S,R),Q)=\begin{cases}-k & \text{if } S<Q,\\ k & \text{if } S>R-Q,\\ 0 & \text{otherwise,}\end{cases}$$

with k a constant. This term is relevant only if it is dominant with respect to the linear one. We thus choose the limit $k\to\infty$, so that the transition probabilities $\tau(1|S)$ are given by

$$\tau(1|S)=\begin{cases}0 & \text{if } S<Q,\\ 1 & \text{if } S>R-Q,\\ \dfrac{1}{1+\exp\{-2[H+Jm(S,R)]\}} & \text{otherwise.}\end{cases}\tag{1}$$

For $Q=0$ we recover the usual heat-bath dynamics for an Ising-like model with reduced Hamiltonian $\mathcal{H}=\Sigma_i V(m_i)\sigma_i$. For $R=3$, $Q=1$ we have the model of Ref. [6] with two absorbing states. The quantities H and J range from $-\infty$ to ∞. For easy plotting, we use $j=[1+\exp(-2J)]^{-1}$ and $h=[1+\exp(-2H)]^{-1}$ as control parameters, mapping the real axis $(-\infty,\infty)$ to the interval $[0,1]$.

The fraction c of 1's (density) in a configuration and the cluster density ρ are defined by

$$c=1L\sum_i s_i \quad\text{and}\quad \rho=\frac{1}{L}\sum_i|s_i-s_{i+1}|.$$

Both the uniform zero state and one state correspond to $\rho\to 0$ in the thermodynamic limit, while the active state corresponds to $\rho>0$.

III. NUMERICAL RESULTS

Let us first review the $R3Q1$ case, whose phase diagram is reported in Fig. 1. A first-order phase transition occurs on the vertical line that ends at a bicritical point where it meets two second-order phase transition curves. In the neighborhood of the first-order phase transition line a typical pattern of the system is composed of large patches of zeros and 1's, separated by disordered zones (walls) whose width does not grow in time. These walls perform a sort of random motion and annihilate in pairs [see Fig. 2(c)]. By lowering J an active, disordered phase appears [see Fig. 2(b)]. The transition between the ordered (absorbing) and disordered (active) phases occurs by destabilization of the width of the walls that percolate in the whole system. In the limit $J=-\infty$ ($j=0$) we have typical chaotic class-3 cellular automata patterns [10], as shown in Fig. 2(a). Damage spreading analysis [6] shows that inside the active phase there is a region in which a variation in the initial configuration can influence the asymptotic configuration. This region may be called chaotic. However, in the mean-field approximation, this region simply corresponds to a stable fixed point of the average density. Indeed,

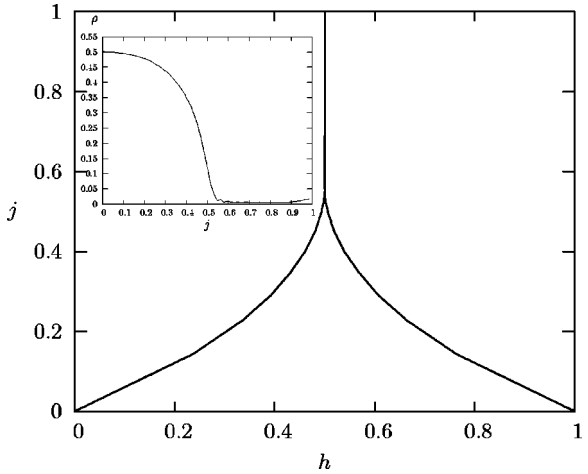

FIG. 1. Phase diagram of $R3Q1$ model. The upper left region corresponds to the absorbing state 0, the upper right region to the absorbing state 1, and the lower region to the disordered phase. In the inset we show the asymptotic value of ρ as a function of j for $H=0$ ($h=0.5$). Here $L=T=10^4$.

the fluctuations of the density remain quite small and a spatial coarse-graining would generate a simple random pattern.

This underlying disorder is revealed also by the asymptotic value of ρ for $H=0$ ($h=0.5$) as a function of j, shown in the inset of Fig. 1. It exhibits a monotonic behavior, with a maximum for $j=0$ (corresponding to the smallest average length of homogeneous clusters) and a continuous phase transition at the bicritical point that separates the active ($\rho>0$) and quiescent ($\rho=0$) phases.

By increasing R, new features appear. Typical patterns are shown in Fig. 3 for different values of j. As illustrated in Fig. 4, ρ is no longer a monotonic function of j, and a new, less disordered region appears inside the active one for small values of j. The transition between the active and the quiescent phases become sharper with increasing R, as shown in Fig. 4.

The pattern shown in Fig. 3(a), is reminiscent of chaotic deterministic cellular automata. We refer to this region as coherently chaotic, since it corresponds to irregular coherent oscillations of large patches of sites. This region of the parameters is dominated by an almost deterministic behavior, and the presence of many metastable absorbing states, revealed by transient regular patterns in Fig. 3(a). As we discuss in Sec. IV, the mean-field analysis gives a chaotic map for large antiferromagnetic values of J, but we were unable to find a clear order parameter that numerically distinguishes this region from the broader chaotic one in which the asymptotic configuration exhibits a dependence on variations in the initial configuration. In Sec. III A, we analyze the chaotic region by means of (finite size) Lyapunov exponents.

By increasing J, the coherent patches shrink and the Lyapunov exponent decreases and finally becomes negative. The system asymptotically loses its dependence on the initial conditions and is dominated by the stochastic components. This phase is termed irregular, and appears completely random. Figure 3(b), shows a typical pattern at the boundary between the chaotic and the irregular phase.

By observing in rapid sequence the patterns generated with increasing values of J, one observes a sudden freezing

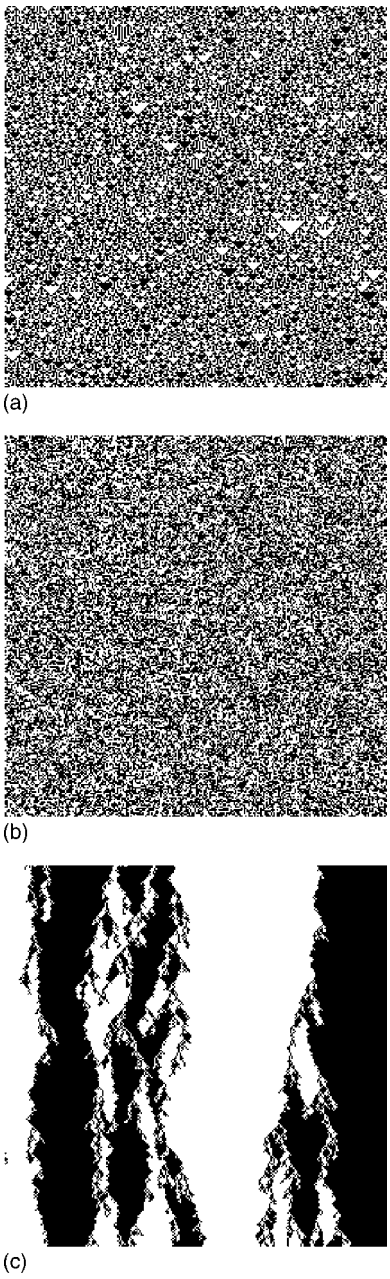

FIG. 2. Typical space time patterns of the $R3Q1$ model for $H=0$ ($h=0.5$) with $L=T=256$. Time increases downward. (a): Chaotic deterministic pattern $j=0.031\,25$. (b): Disordered phase $j=0.5$. (c): Competition between quiescent phases $j=0.546\,88$ (first-order transition).

of the (random) image, just before the transition between the active and quiescent phases, corresponding to Fig. 3(c). This effect is due to the insensitivity of the patterns not only to the initial condition, but also to the parameters (see Sec. III B). We term this phase disordered.

Finally, the quiescent phase is asymptotically dominated by the two absorbing states, with the usual annihilating wall dynamics, Fig. 3(d).

Figure 4 shows that the active-quiescent transition becomes sharper when R is increased, and that the cluster density exhibits a cusp at the transition. By enlarging this region

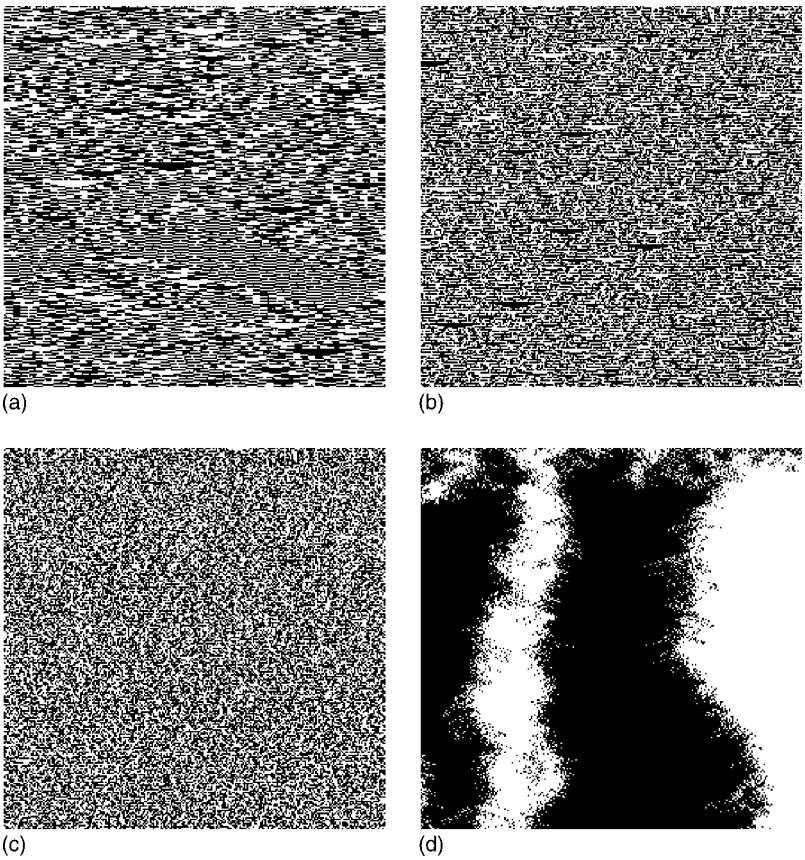

FIG. 3. Typical space time patterns ($L=T=256$) for model $R11Q1$ and $H=0$, starting from a disordered initial condition with $\rho_0=0.5$. (a), $j=0.056\,250$, A: Coherently chaotic phase. One can observe rare triangles with base larger that R, corresponding to the unstable absorbing states, and other metastable patterns, corresponding to additional absorbing states for $J\to-\infty$. (b), $j=0.421\,875$, B: At the boundary between the chaotic and the irregular phases, the only locally absorbing states are (rare) patches of 0 and 1. Most of the pattern looks random, with some triangles reminiscent of chaotic CA. (c), $j=0.478\,125$, C: Disordered phase. The pattern looks random and the difference between patterns obtained with different values of the parameters (and the same random numbers) is vanishing. (d), $j=0.562\,500$, D: Quiescent phase. In this phase the only stable states are the absorbing ones. The boundaries separating the phases move randomly until coalescence.

one sees that for $H=0$ (Fig. 5) the cluster density exhibits two sharp bends, while for $H=0.42$, (Fig. 6), only one bend is present. This is reminiscent of the universality class change (parity conservation, DP) for $H=0$, $H\neq 0$, respectively, in the $R3Q1$ model [6]. Notice also that the irregular-disorder transition at $j\simeq 0.494$ is rather peculiar, since ρ first decreases and then suddenly jumps to high values.

The bends are not finite size or time effects. As shown in Fig. 3(c), in this range of parameters the probability of observing a local absorbing configuration (i.e., patches of zeros or 1's) is vanishing. All other local configurations have finite probability of originating zeros or 1's in the next time step. The observed transitions are essentially equivalent to those of an equilibrium system, which in one dimension and for short-range interactions cannot exhibit a true phase transi-

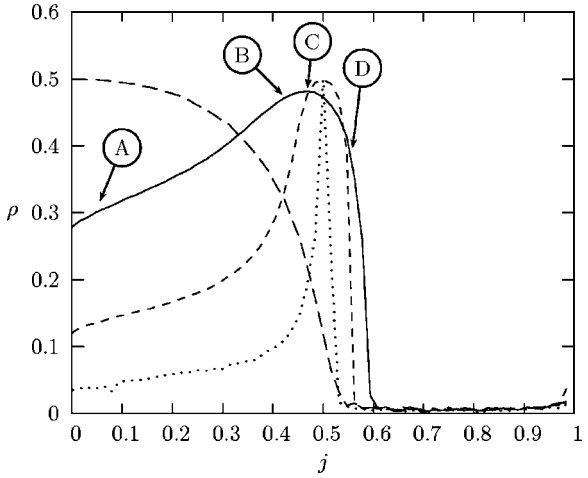

FIG. 4. Behavior of ρ for $H=0$. $R3Q1$ (long dashed), $R11Q1$ (solid), $R41Q1$ (dashed), and $R81Q1$ (dotted). Letters correspond to patterns in Fig. 3.

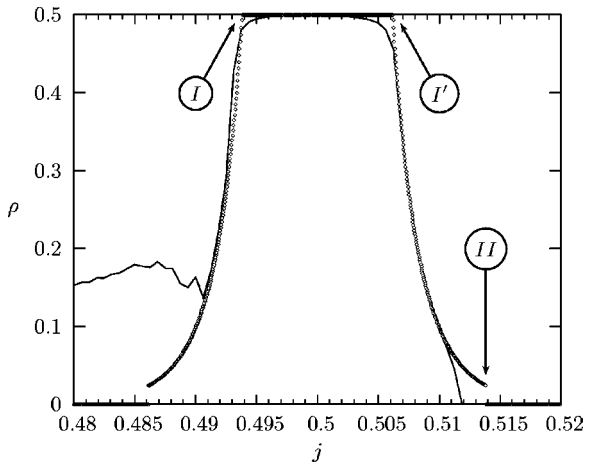

FIG. 5. Comparisons between numerical (thin line) and mean-field (thick, dotted line) results for $R81Q1$ and $H=0$ ($h=0.5$). The estimated critical values are $j_{\mathrm{I}}^{*}\simeq 0.493\,827$, $j_{\mathrm{I}}^{*}\simeq 0.506\,173$, and $j_{\mathrm{II}}^{*}\simeq 0.513\,84$. This figure has been obtained with much larger simulations of the corresponding line in Fig. 4, and more details emerge. The patterns shown in Fig. 3 (which however refer to $R=11$) illustrate the typical behavior of the system to the left (B), in the middle (C), and to the right (D) of the plateau.

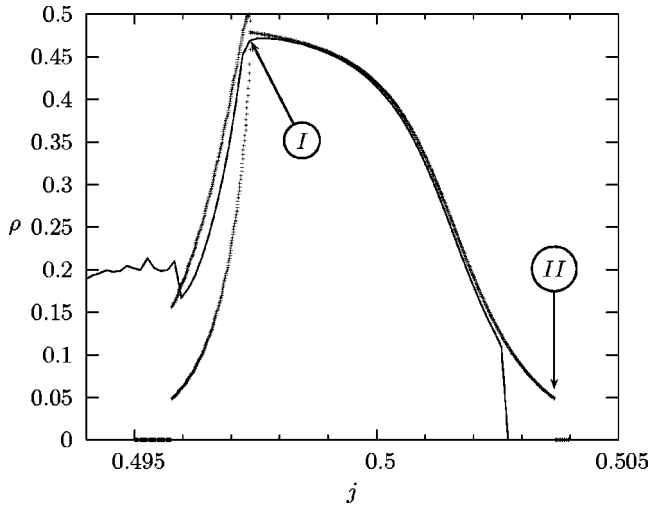

FIG. 6. Comparisons between numerical (thin line) and mean-field (thick, dotted line) results for $R201Q5$ and $H=0.42$ ($h=0.7$). The two sets of pluses mark the period-2 region. The estimated critical values are $j_{\mathrm{I}}^{*}\simeq 0.497\,40$ and $j_{\mathrm{II}}^{*}\simeq 0.503\,69$.

tion. The bends thus become real salient points only in the limit $R\to\infty$.

Our simulations were carried out using the fragment method [11], in which a set of configurations (replicas) are updated with different values of parameters using the same random numbers, and the same initial configuration.

A. Chaos and Lyapunov exponent in cellular automata

State variables in cellular automata are discrete, and thus the usual linear stability analysis classifies them as stable systems. The occurrence of disordered patterns and their propagation in stable dynamical systems can be classified into two main groups: *transient chaos* and *stable chaos*.

Transient chaos is an irregular behavior of finite lifetime characterized by the coexistence in the phase space of stable attractors and chaotic nonattracting sets, namely, chaotic saddles or repellers [12]. After a transient irregular behavior, the system generally collapses abruptly onto a nonchaotic attractor. This kind of behavior is reminiscent of some class-4 (nonchaotic) deterministic cellular automata (DCA's) [10], and can be present in continuous systems having a discrete dynamics as a limiting case [13].

Stable chaos constitutes a different kind of transient irregular behavior [14,15] which cannot be ascribed to the presence of chaotic saddles and therefore to divergence of nearby trajectories. Moreover, the lifetime of this transient regime may scale exponentially with the system size (super-transients as defined in Refs. [14,15]), and the final stable attractor is practically never reached for large enough systems. One is thus allowed to assume that such transients may be of substantial experimental interest and become the only physically relevant states in the thermodynamic limit.

The emergence of this chaoticity in class-3 (chaotic) DCA dynamics is effectively illustrated by a damage spreading analysis [16,17], which measures the sensitivity to initial conditions and for this reason is considered as the natural extension of the Lyapunov technique to discrete systems. In this method, indeed, one monitors the behavior of the distance between two replicas of the system evolving from slightly different initial conditions, or the speed of propagation of a disturbance [18]. The dynamics is considered unstable and the DCA is called chaotic, whenever a small initial difference between replicas spreads through the whole system. On the contrary, if the initial difference eventually freezes or disappears, the DCA is considered nonchaotic.

Due to the limited number of states of the automaton, damage spreading does not account for the maximal production of uncertainty, since the two replicas may synchronize locally just by chance (self-annihilation of the damage). Moreover, there are different definitions of damage spreading for the same rule [19].

To better understand the nature of the active phase, and up to what extent it can be denoted chaotic, we extend the finite-distance Lyapunov exponent definition [20] to probabilistic cellular automata. A similar approach has been used in Ref. [21], calculating the Lyapunov exponents of a Kauffman random Boolean network in the annealed approximation. As shown in that paper, this computation gives the value of the (classic) Lyapunov exponent obtained by the analysis of time-series data using the Wolf algorithm [22].

Given a Boolean function $f(x,y,\ldots)$ $(x,y,\cdots\in\{0,1\})$, we define the Boolean derivative $\partial f/\partial x$ with respect to x by

$$\frac{\partial f}{\partial x}=\begin{cases}1 & \text{if } f(|x-1|,y,\ldots)\neq f(x,y,\ldots),\\ 0 & \text{otherwise},\end{cases} \tag{2}$$

which represents a measure of sensitivity of a function with respect to x. The evolution rule of a probabilistic cellular automation can be written as

$$x_i^{t+1}=\begin{cases}1 & \text{if } r<\tau(1|S_i^t),\\ 0 & \text{otherwise},\end{cases}$$

where r is a random number uniformly distributed in [0, 1]. The Boolean derivative with respect to x_j is evaluated by using the same r in the comparison implied in Eq. (2).

For a PCA, we can thus build the Jacobian matrix $J_{ij}=\partial x_i^{t+1}/\partial x_j^t$, $i,j=0,\ldots,L-1$, by taking the derivatives over the configurations generated by the dynamics (the trajectory of the system). The maximum Lyapunov exponent λ can now be defined in the usual way as the expansion rate of a tangent vector $\boldsymbol{v}(t)$, whose time evolution is given by

$$\boldsymbol{v}(t+1)=\boldsymbol{J}\boldsymbol{v}(t).$$

When all the components of $\boldsymbol{v}$ become zero, $\lambda=-\infty$ and no information about the initial configuration may *percolate* as $t\to\infty$ [20]. This maximum Lyapunov exponent is also related to the synchronization properties of cellular automata [23].

A preliminary computation of λ for our model is reported in Fig. 7. It can be noticed that the boundary $j_c(R)$ of $\lambda\geqslant 0$ is not monotonic with R, reaching a maximum value for $R\simeq 11$. By comparison with Fig. 4, one can see that the chaotic phase is included in the irregular one.

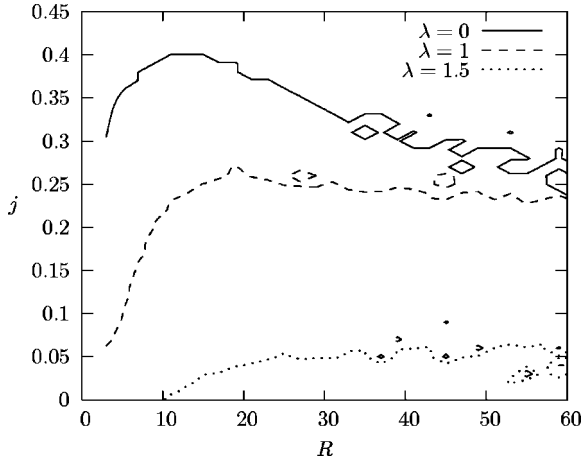

FIG. 7. Contour plot of the maximum Lyapunov λ exponents for different values of R and j, for $H=0$. The solid line represents the boundary between the $\lambda \geqslant 0$ and $\lambda = -\infty$ phases. Data obtained from simulations with $L=2000$ and $T=500$.

B. Parameter dependence

We can numerically characterize the irregular-disorder transition by looking at the sensitivity of space-time patterns with respect to the variations of parameters. Using the fragment method [11] a set of configurations (replicas) are updated with different values of parameters using the same random numbers, i.e., with the same disordered field and initial conditions. The quantity

$$\chi(J) = \lim_{\Delta j \to 0} \lim_{t \to \infty} \sum_i |s_i^t(J + \Delta J) - s_i^t(J)|$$

is a measure of the susceptibility. For large correlations one expects very small differences among replicas. As shown in Fig. 8, this susceptibility is strongly anticorrelated to the average number of clusters ρ. This is rather surprising since the pattern in Fig. 3(c), is absolutely irregular. We can state the problem in terms of the dependence of the asymptotic configuration on three factors: the initial configuration, the parameters J and/or H (which includes the dependence on temperature), and the disordered field (the random numbers).

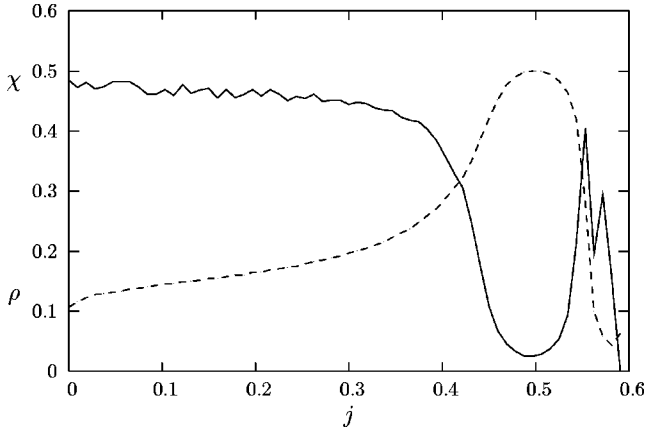

FIG. 8. Susceptibility χ (continuous line) and average number of clusters ρ (dashed line) for $R11Q1$, $H=0$, $\Delta j=0.01$.

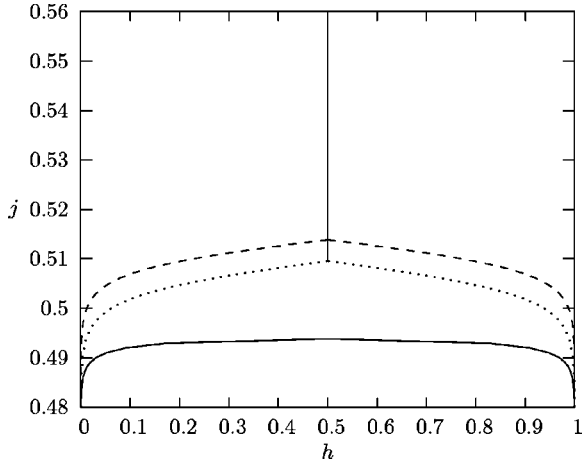

FIG. 9. Mean-field phase diagram for $R=81$. The upper curves correspond to the transition II from the quiescent to the disordered phases, $R81Q5$ (dashed) and $R81Q1$ (dotted). The solid curve corresponds to the transition I from the disordered to the irregular phase.

Every phase in that figure represents a different kind of dependence: in the chaotic phase, the asymptotic configuration experiences the dependence on all three factors. This is analogous to the *damage spreading* phase in the Domany-Kinzel model [16,17,19]. In the nonchaotic region the asymptotic configuration depends only on the choice of random numbers and on the parameters and temperature used in the simulation. The quantity χ measures the actual dependence on this latter factor, and the disordered phase might be denoted the *temperature-independent* phase. Finally, the ordered phase is essentially independent of all factors, except in the vicinity of the phase boundary. As shown in the next section, this behavior is understandable in the context of a field-theoric approximation.

IV. MEAN-FIELD APPROXIMATION

In the simplest mean-field approximation, the density c evolves in time according to

$$c(t+1) = \sum_{S=0}^{R} W^{(R,S)}(c(t))\tau(1|S), \tag{3}$$

with

$$W^{(R,S)}(c) = \binom{R}{S} c^S (1-c)^{R-S}.$$

An example of a mean-field phase diagram is reported in Fig. 9.

For large R, $W^{(R,S)}$ can be approximated by

$$W^{(R,S)}(c) \simeq \frac{1}{\sqrt{2\pi c(1-c)R}} \exp\left[-\frac{R(S/R-c)^2}{2c(1-c)} \right], \tag{4}$$

and the summation can be replaced by an integral. The parameters of the resulting equation may be rescaled by using $\tilde{J}=JR$ and $\tilde{Q}=Q/R$. In the limit $R \to \infty$ ($\tilde{J}$ and $\tilde{Q}$ fixed), $c(t+1)=f(c(t);H,\tilde{J})$ with

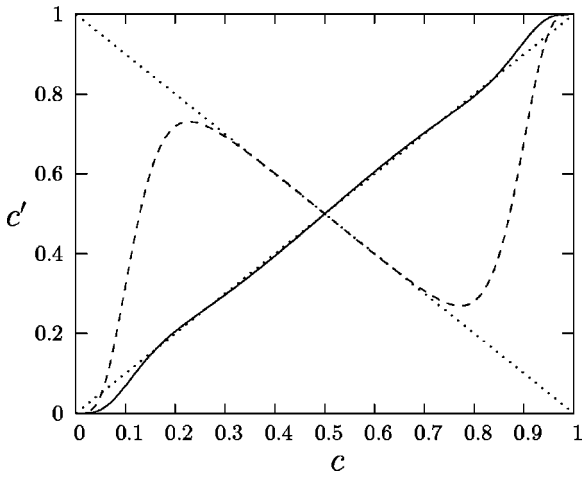

FIG. 10. Mean-field map Eq. (3) in the neighborhood of transitions I ($\tilde{J}\simeq -1$, dashed line) and II ($\tilde{J}\simeq 1$, solid line), for $H=0$ and $\tilde{Q}=0.02$.

$$f=\begin{cases}0 & \text{if } c<\tilde{Q},\\ 1 & \text{if } c>1-\tilde{Q},\\ \dfrac{1}{1+\exp[-2(H+\tilde{J}(2c-1))]} & \text{otherwise.}\end{cases} \tag{5}$$

The requirement of constant rescaled variables means that the variation of J for large R triggers large variations of $\tilde{J}$, and consequently the transition region becomes sharper.

This approximation is expected to be particularly good in the disordered phase, i.e., for J, $H\simeq 0$, as shown in Fig. 5. In the finite-dimensional case, one has to add a noise term, representing the influence of neighboring sites, whose amplitude is of the order of the width of the Gaussian in Eq. (4), $\sqrt{c(1-c)/R}$. In this region, the density c and the cluster density ρ are related by $\rho=2c(1-c)$.

For J, $H\simeq 0$ the mean-field approximation gives a stable fixed point $c^*(H,\tilde{J})\neq 0,1$ for the density, which assumes the maximum value $c^*=0.5$ for $J=H=0$.

The origin of the irregular-disordered and disorder-quiescent phase transitions marked by I and II, respectively, in Figs. 5 and 6 is related to the loss of stability of the mean-field fixed point $c^*\neq 0,1$ [see Eq. (5) and Fig. 10].

The transition I is given by

$$c_{\mathrm{I}}^*=f(c_{\mathrm{I}}^*;H,\tilde{J}),\qquad \left.\frac{df(c;H,\tilde{J})}{dc}\right|_{\mathrm{I}}=-1, \tag{6}$$

which would induce a period-doubling cascade in the mean-field approximation (disregarding the presence of absorbing states). The solution of Eqs. (6) is

$$c_{\mathrm{I}}^*=\frac{1}{2}(1+\sqrt{1+\tilde{J}^{-1}}),$$

$$H_{\mathrm{I}}^*=-\tilde{J}\sqrt{1+\tilde{J}^{-1}}-\frac{1}{2}\ln\left(\frac{1-\sqrt{1+\tilde{J}^{-1}}}{1+\sqrt{1+\tilde{J}^{-1}}}\right).$$

The critical value J_{I}^* can be obtained numerically once given the value of $H^*=H^*(J^*)$, and corresponds to the left bend in Figs. 5 and 6.

For $H=0$ (Fig. 5) the period-doubling instability brings the local configuration into an absorbing state, and the lattice dynamics is therefore driven by interactions among patches which are locally absorbing. This essentially corresponds to the dynamics of a deterministic cellular automaton of chaotic type, i.e., a system that is insensitive to infinitesimal perturbations but reacts in an unpredictable way to finite perturbations [13]. In other words, in this region the original stochastic model behaves like a chaotic deterministic one after a coarse-graining of patches. We expect that this correspondence will become more and more exact with growing R. From a field-theoretical point of view this means that the renormalization flux tends toward a chaotic model instead of the usual fixed-point dynamics.

For $H=0.42$, as shown in Fig. 6, the period-2 phase has a finite amplitude, before falling into the DCA-like dynamics by reducing J.

For $H=0$, one can check that the critical value $J_{\mathrm{I}'}^*$ for which $df/dc=1$ (the right boundary of the disordered phase) is given by $J_{\mathrm{I}'}^*=-J_{\mathrm{I}}^*$. In terms of j, it means that the disordered phase is located symmetrically with respect to $j=0.5$, as confirmed by Fig. 5.

The disordered phase corresponds to random space-time patterns [Fig. 3(c)] and thus accurate mean-field predictions. It is characterized by a stable fixed point for the density $c=0.5$ (completely disordered configurations). This implies $\rho=0.5$, and, using Eq. (5), implies insensitiveness to J. This corresponds to the low values of the susceptibility χ shown in Fig. 4. It also implies vanishing correlations and vanishing variance of the order parameter.

For $J>0$ (transition II) we have

$$c_{\mathrm{II}}^*=f(c_{\mathrm{II}}^*;H,\tilde{J})=\begin{cases}\tilde{Q},\\ 1-\tilde{Q},\end{cases}$$

and thus the critical value J_{II}^* is

$$J_{\mathrm{II}}^*=\frac{1}{2\tilde{Q}-1}\left[\pm H+\frac{1}{2}\ln\left(\frac{\tilde{Q}}{1-\tilde{Q}}\right)\right].$$

Once a portion of the lattice has been attracted to an absorbing state, it pulls the neighboring regions to this same state, due to the ferromagnetic ($J>0$) coupling.

This approximation, disregarding fluctuations, overestimates the critical value J_{II}^*, as shown in Figs. 5 and 6.

We analyze extensively the mean-field behavior of the system for $H=0$ and $J=-\infty$. As shown in Fig. 11, for a given value of R, there is always a critical Q_c value of Q for which the active phase disappears, with an approximate correspondence $Q_c\simeq 2/5R$. One can also observe that the chaotic oscillations of the mean-field map, which roughly correspond to the coherent-chaotic phase of the model, appear only for

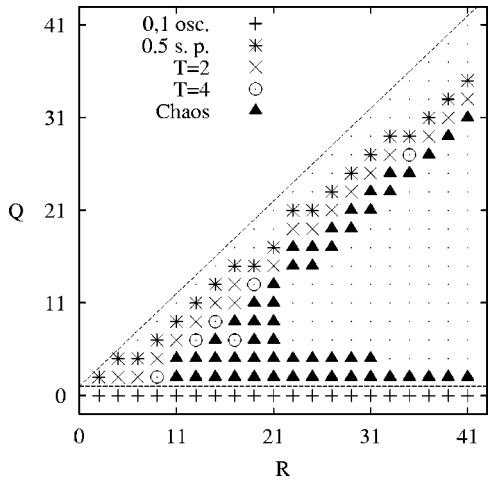

FIG. 11. Case $H=0$, $J=-\infty$: the mean-field R-Q phase diagram of the mean-field approximation. Points mark parameter values for which the absorbing states are the only stable attractors. A plus sign denotes period-2 temporal oscillations between absorbing states, a star denotes the presence of a stable point at $c=0.5$, a cross (circle) denotes period-2 (4) oscillations between two nonzero and non-1 densities, and triangles denote chaotic oscillations.

large values of R. Since the absorbing states are always present, their chaotic oscillations may bring the system into the quiescent phase, as shown by the hole to the right of the triangles in Fig. 11.

The correspondence between the chaotic behavior of the mean-field approximation and the actual behavior of the system will be the subject of a future work.

V. CONCLUSIONS

We have investigated a general one-dimensional model with extended-range interactions and symmetric absorbing states. The model is characterized by competing ferromagnetic linear and antiferromagnetic nonlinear coupling.

By means of numerical simulations and mean-field approximations we have shown that a chaotic phase is present for strong antiferromagnetic coupling. This phase may be identified as a stable-chaotic region, in which the behavior of the (originally stochastic) system is essentially deterministic and its behavior is highly irregular and essentially unpredictable. The mean-field map exhibits a chaotic behavior for a large interaction range R, and this behavior is reflected in the appearance of many metastable states in the system, for extremely strong antiferromagnetic coupling.

A disordered phase, insensitive to parameter variations, appears at the boundary between the active and the quiescent ones, and the transitions appear to be of equilibrium type, i.e., truly salient points only in the limit $R\to\infty$.

We expect that in higher dimensions one can recover some aspects of these phase transitions without imposing the presence of absorbing states, i.e., using finite couplings.

ACKNOWLEDGMENTS

Partial economic support from Project No. IN109602 DGAPA-UNAM and the Coordinación de la Investigación Científica UNAM is acknowledged. F.B. and F.F. acknowledge partial support from the PRIN2003 project "Order and Chaos in Nonlinear Extended Systems" funded by MIUR, Italy.

APPENDIX: EQUIVALENCE BETWEEN DYNAMIC ISING MODEL AND CELLULAR AUTOMATA

As an illustration, we present here a derivation of the equivalence of the kinetic Ising model (here we choose the heat bath) with a cellular automaton (the Domany-Kinzel model) in order to elucidate the role of infinite coupling parameters and absorbing states. This derivation is similar to that of Ref. [1] but more general.

The Ising model is defined by the couplings among spins. The configuration at time t is denoted as $\boldsymbol{\sigma}=\sigma_1,\sigma_2,\ldots$ and the configuration at time $t+1$ as $\boldsymbol{\sigma}'=\sigma_1',\sigma_2',\ldots$. Let us write the temperature-dependent Hamiltonian as

$$\mathcal{H}(\boldsymbol{\sigma})=\sum_i H(\sigma_{i-1},\sigma_i\sigma_{i+1}),$$

with

$$H(x,w,y)=J^{(0)}w+J^{(1)}xw+J^{(2)}wy+J^{(3)}xwy. \quad \text{(A1)}$$

The transition probabilities τ must obey the detailed balance condition

$$\frac{\tau(\boldsymbol{\sigma}'|\boldsymbol{\sigma})}{\tau(\boldsymbol{\sigma}|\boldsymbol{\sigma}')}=\exp[\mathcal{H}(\boldsymbol{\sigma}')-\mathcal{H}(\boldsymbol{\sigma})].$$

In each step we can update in parallel all even or odd sites, obtaining

$$\frac{\tau(\boldsymbol{\sigma}'|\boldsymbol{\sigma})}{\tau(\boldsymbol{\sigma}|\boldsymbol{\sigma}')}=\prod_i \frac{\tau(\sigma_{i-1},\sigma_i',\sigma_{i+1}|\sigma_{i-1},\sigma_i,\sigma_{i+1})}{\tau(\sigma_{i-1},\sigma_i,\sigma_{i+1}|\sigma_{i-1},\sigma_i',\sigma_{i+1})},$$

where the product is restricted to either even or odd sites. The detailed balance condition can thus be satisfied locally. Choosing the heat-bath dynamics

$$\tau(x,1,y|x,w,y)=\frac{\exp[-H(x,1,y)]}{\exp[-H(x,-1,y)]+\exp[-H(x,1,y)]}$$

the transition probabilities do not depend on the present value of the spin $w=\sigma_i^t$ so that the lattice (with even or infinite lattice sites) may be decoupled into two noninteracting sublattices with the same geometry of the DK model. From now on, to be coherent with the usual cellular automaton notation, we shall express the transition probabilities in terms of the Boolean variables $s_i=(\sigma_i+1)/2$, and we shall denote the local field as $h(a,b)\equiv H(2a-1,1,2b-1)$.

Let us denote the DK transition probabilities $\tau(s_i'|s_{i-1},s_{i+1})$ as

$$\tau(1|00)=\varepsilon,\quad \tau(1|01)=\tau(1|10)=p,\quad \tau(1|11)=q.$$

We get for the heat-bath dynamics

$$\tau(1|ab)=\frac{1}{1+\exp[-2h(a,b)]}$$

and thus

$$h(a,b) = \frac{1}{2} \ln \frac{\tau(1|ab)}{1-\tau(1|ab)}.$$

Substituting into Eq. (A1) one obtains a linear system,

$$J^{(0)} - J^{(1)} - J^{(2)} + J^{(3)} = \frac{1}{2} \ln \frac{\varepsilon}{1-\varepsilon},$$

$$J^{(0)} + J^{(1)} - J^{(2)} - J^{(3)} = \frac{1}{2} \ln \frac{p}{1-p},$$

$$J^{(0)} - J^{(1)} + J^{(2)} - J^{(3)} = \frac{1}{2} \ln \frac{p}{1-p},$$

$$J^{(0)} + J^{(1)} + J^{(2)} + J^{(3)} = \frac{1}{2} \ln \frac{q}{1-q}.$$

Finally, we have

$$J^{(0)} = \frac{1}{8} \ln \frac{\varepsilon}{1-\varepsilon} + \frac{1}{8} \ln \frac{q}{1-q} + \frac{1}{4} \ln \frac{p}{1-p},$$

$$J^{(1)} = J^{(2)} = -\frac{1}{8} \ln \frac{\varepsilon}{1-\varepsilon} + \frac{1}{8} \ln \frac{q}{1-q},$$

$$J^{(3)} = \frac{1}{8} \ln \frac{\varepsilon}{1-\varepsilon} + \frac{1}{8} \ln \frac{q}{1-q} - \frac{1}{4} \ln \frac{p}{1-p}.$$

In the limit $\varepsilon \to 0$ all couplings become infinite.

[1] A. Georges and P. Le Doussal, J. Stat. Phys. **54**, 1011 (1989).
[2] W. Kinzel and E. Domany, Phys. Rev. Lett. **53**, 311 (1984); W. Kinzel, Z. Phys. B: Condens. Matter **58**, 229 (1985); in *Percolation Structures and Processes*, edited by G. Deutsch, R. Zallen, and J. Adler (Adam Hilger, Bristol, 1983).
[3] M. Mézard, G. Parisi, and M. A. Virasoro, *Spin Glass Theory and Beyond* (World Scientific, Singapore, 1987); K. H. Fischer and J. A. Hertz, *Spin Glasses* (Cambridge University Press, Cambridge, England, 1991).
[4] D. J. Gross and M. Mézard, Nucl. Phys. B **240**, 431 (1984); E. Gardner, *ibid.* **257**, 747 (1985).
[5] F. Bagnoli, F. Franci, and R. Rechtman, in *Cellular Automata*, edited by S. Bandini, B. Chopard, and M. Tomassini (Springer-Verlag, Berlin, 2002), p. 249.
[6] F. Bagnoli, N. Boccara, and R. Rechtman, Phys. Rev. E **63**, 046116 (2001).
[7] H. Hinrichsen, Phys. Rev. E **55**, 219 (1997).
[8] H. K. Janssen, Z. Phys. B: Condens. Matter **42**, 152 (1981).
[9] P. Grassberger, Z. Phys. B: Condens. Matter **47**, 365 (1982).
[10] S. Wolfram, Physica D **10**, 1 (1984).
[11] F. Bagnoli, P. Palmerini, and R. Rechtman, Phys. Rev. E **55**, 3970 (1997).
[12] T. Tel, in *Proceedings of the 19th IUPAP International Conference on Statistical Physics*, edited by Hao Bai-lin (World Scientific Publishing, Singapore, 1996).
[13] F. Bagnoli and R. Rechtman, Phys. Rev. E **59**, R1307 (1999); F. Bagnoli and F. Cecconi, Phys. Lett. A **260**, 9 (2001), and references therein.
[14] J. P. Crutchfield and K. Kaneko, Phys. Rev. Lett. **60**, 2715 (1988), K. Kaneko, Phys. Lett. A **149**, 105 (1990).
[15] A. Politi, R. Livi, G.-L. Oppo, and R. Kapral, Europhys. Lett. **22**, 571 (1993).
[16] P. Grassberger, J. Stat. Phys. **79**, 13 (1995).
[17] F. Bagnoli, J. Stat. Phys. **79**, 151 (1996).
[18] *Theory and Application of Cellular Automata*, edited by S. Wolfram (Addison-Wesley, Reading, MA, 1986).
[19] H. Hinrichsen, J. S. Weitz, and E. Domany, J. Stat. Phys. **88**, 617 (1997).
[20] F. Bagnoli, R. Rechtman, and S. Ruffo, Phys. Lett. A **172**, 34 (1992).
[21] B. Luque and R. V. Solé, Physica A **284**, 33 (2000).
[22] A. Wolf, J. B. Swift, H. L. Swinney, and J. A. Vastano, Physica D **16**, 285 (1985).
[23] F. Bagnoli and R. Rechtman, Phys. Rev. E **59**, R1307 (1999).